# University of Huddersfield Repository

Muller, Matthias, Barrans, Simon and Blunt, Liam

Predicting Plastic Deformation and Work Hardening during V-Band Formation

## Original Citation

This version is available at http://eprints.hud.ac.uk/id/eprint/9791/

http://eprints.hud.ac.uk/

# Predicting Plastic Deformation and Work Hardening during V-Band Formation

M. Muller [a] (*m.muller@hud.ac.uk*), S. M. Barrans[b] (*s.m.barrans@hud.uk.ac*), L. Blunt[b],

(*l.a.blunt@hud.ac.uk*)

a,b Centre for Precision Technologies CPT, School of Computing & Engineering, University of Huddersfield, Queensgate, Huddersfield, HD1 3DH, UK,

a Tel. 01484 47 3917

**Abstract:** V-Band Clamps are manufactured using a cold roll forming process consisting of six passes which plastically deform an initially flat strip by bending to produce the band's V-section. In this paper a new method of validating numerically predicted plastic deformation in a cold formed metal strip is presented. Tensile testing of samples of the band's material was used to obtain a direct link between plastic strain and work hardness of this particular material. Using this correlation, the equivalent plastic strain (PEEQ) values predicted by finite element simulations were converted into hardness values. These values were compared to experimental work, in which samples of each pass of the roll forming process were taken to determine the work hardness in the cross section of the V-band using a micro-hardness machine. The error in strain predicted by the numerical method and hardness obtained by testing was found to be between 0.4% and 16.9%. This error was mainly due to uncertainty in material properties and the accuracy of the measurement technique. Compared to the more classical approach of measuring strain distribution with strain gauges, this method is more precise and accurate, as it is able to pick up even small changes in strain distribution.

**Keywords:** V-Band, Plastic Deformation, Work Hardening, Finite Element Analysis, Roll Forming Process

# 1   Introduction

V-band clamps are widely used in the automotive, aircraft and aerospace industries to connect a pair of circular flanges to provide a joint with good axial strength and torsional rigidity. Offering the benefit of generating a fluid tight seal joint, they are used to clamp together the housings of turbochargers. Despite their well established benefits and wide use, there is still a lack of published knowledge about the working principle and behaviour of V-band clamps. Some work regarding the working principle of V-bands was originally presented by Mountford (1980) and more recently by Shoghi (2003). In the latter work the author presented a theoretical model able to predict the stresses and forces generated as the clamp is tightened around a pair of flanges. This was validated by Shoghi et al. (2004) using experimental data and Shoghi et al. (2003) using finite element analysis*. The finite element work was developed further by Shoghi et al. (2006) to account for friction in the axial direction when tightening the T-bolt nut and applying an axial load. More recently Barrans and Muller (2009) and Muller and Barrans (2010) have analysed the ultimate axial load capacity of V-band clamps using the finite element method. However, it was partially recognised in this previous work that prediction of the ultimate axial load capacity of V-band joints would require knowledge of the state of the band material. This knowledge is essential if additional plastic deformation generated during joint failure is to be predicted and required an investigation of the manufacturing process. V-band clamps are made of austenitic stainless steel and manufactured using a cold roll forming process. In the first stage an initial flat band-strip is deformed using six passes to form the V-section. The second stage consists of a cold roll-bending process in which the band gets its circular shape as shown in Figure 1.
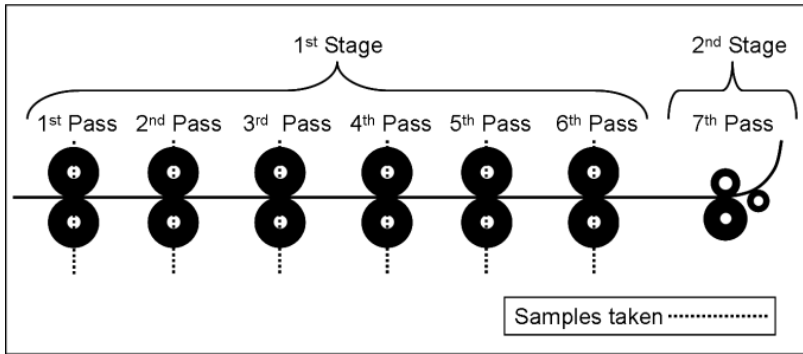
Figure 1: 2 dimensional schematic of rolling process including 1st stage of forming the V-section and 2nd stage of forming circular shape

Several authors have already investigated and numerically predicted similar cold roll forming processes, but have mainly focussed on longitudinal strain effects and the validation of these numerical models, as they have a large impact on wave edges, longitudinal curvature and end flare, hence reducing the quality of the metal strip.

One of the first computer aided simulations of a roll forming process allowed, Kiuchi and Koudabashi (1984) to optimise the production of circular tubes. The simulation enabled them to prevent the occurrence of edge waves, and it ensured that the energy dissipated in each roll pass was equal. McClure and Li (1995) analysed a roll forming process with three passes using a three dimensional finite element model, and validated their investigation by measuring the strain with strain gauges, bonded to the upper and lower surface of the strip. Another three dimensional finite element prediction of a U-shaped cold roll forming process consisting of three passes was undertaken by Heislitz et al. (1996). They found a continuous rise of longitudinal strain in the strip just ahead of each roll stand and comparison of their numerical work to previous experiments showed an approximate deviation of 10%. Around the same time Panton et al. (1996) also predicted the strain distribution in a cold roll forming process. Experiments using strain gauge rosettes showed an increase of longitudinal strain on the strip surface before each roll stand, and a drop after each roll stand, and a continuous increase in shear strain throughout the forming process. From their finite element work, Hong et al. (2001) conclude that the work-hardening exponent has a significant effect on the forming length. The authors claim that a highly work-hardened strip has a shorter forming length, and an annealed strip has a longer. Numerical data for the longitudinal stress was compared to experiments, in which there was good correlation only for the first out of three roll stands.

Lindgren (2005) predicted the longitudinal membrane strain in the flange of a metal strip roll formed in a process consisting of six roll stands. The results correlated very well with those of Heislitz et al. (1996). In their numerical investigation on edge buckling of a roll forming process producing a symmetric channel section, Tehrani et al. (2006) validated their numerical results with strain gauge analysis and agreed with McClure and Li (1995) that the strain is positive/ tensile in the flange, and negative/ compressive in the web. From the three dimensional finite element simulation of Bui and Ponthot (2008) it can be observed that the product quality of the rolled strip significantly depends on the yield limit and work-hardening exponent, this latter conclusion being close to the findings of Hong et al. (2001). For the first time, Zeng et al. (2009) introduced the response surface method to optimise the design of cold roll formed profiles. Employing a finite element model to predict the maximum edge longitudinal membrane strain, the method enabled the authors to reduce the roll passes from six to four, which, as they concluded, saves money and time. Paralikas et al. (2009) developed a model to predict the effect of major process parameters on the quality characteristics of a V-section profile. The characteristics that they mainly focussed on were elastic, and longitudinal residual strains. This work is particularly interesting, as it discusses the possibility of using a simulation of the whole manufacturing chain of the roll forming process to predict the development and transmission of residual strains. Based on their work, Paralikas et al. (2010) introduced an optimisation procedure to improve the quality of the product and reduce costs. Selecting the optimum major process parameters, they managed to reduce longitudinal strains by up to 20-35%, and shear strains by up to 30-50%. Han et al. (2002) also investigated a multi-stand cold roll forming process, but by using the finite strip rather than the finite element method. They, too, mainly analysed the development of longitudinal strains throughout the process. This model was employed by Han et al (2005) to investigate the effect of forming parameters on the peak longitudinal edge membrane strain development. Zhang et al. (2010) introduced a finite strip model in which the stiffness and transition matrix have been improved. Proving the accuracy of the method by predicting the longitudinal strain, the authors claim that their results are more applicable. One phenomenon that has been found by all authors mentioned so far is that the peak longitudinal strain occurs just ahead of the roll stand. McClure and Li (1995) showed that the maximum strain is a function of fold angle, whereas Han et al (2005) proved that increasing the bend angle increment, the strip thickness, the flange length, the distance between roll stands, and the web width increased the peak longitudinal edge membrane strain. Zhu et al (1996) claim that the peak longitudinal strain increases with a larger material thickness and bend angle. Han et al (2005) and Lindgren (2007a) agree that increasing the material yield limit decreases the longitudinal membrane

strain. Paralikas et al. (2009) identified several other parameters to be influential to the longitudinal strain peak. Bhattacharyya et al. (1984) and based on their work Lindgren (2007b), have mathematically analysed a cold roll forming process. Whilst all of the work discussed so far has helped understanding of forming processes, none of the work has taken into account stress and strain distributions through the thickness of the formed metal sheet. Moreover, the roll forming processes investigated have only focussed on sheets with a very large width to thickness ratio, in which shear stress effects can almost be neglected. The exception is Paralikas et al. (2010), who showed that reducing shear stress by up to 50% can significantly increase the quality of the roll formed product, and Panton et al. (1996) who showed a continuous increase of shear strain throughout the roll forming process.

Residual stresses in cold formed products have been studied by Weng and Pekoz (1990) for channel sections, Weng and White (1990a and 1990b) for thick steel plates, and Kleiner and Homburg (2004) for sheet metal forming. These authors have all applied either the hole-drilling or sectioning technique using strain gauges to measure residual strains. The latter technique was also used by Cruise and Gardner (2008) who stated that this is the better method when testing stainless steel. Quach et al. (2006) have numerically investigated residual stresses through the thickness of press-baked thin-walled sections, but only validated their finite element model by comparing outer surface and peak compressive stresses. It is very well understood that stainless steel can be work hardened as demonstrated by Hong et al. (2001) and Kain et al. (2004). Kumar et al. (2004) and Milad et al. (2008) state that for austenitic stainless steel unstable austenite partially transforms into martensite, greatly increasing the mechanical strength and hardness. Kim et al. (2007) have studied exactly this relation and their results showed good agreement between numerically predicted plastic strain and experimentally obtained hardness values.

Despite cold roll forming processes being studied so extensively, none of the work presented here has managed to accurately measure the plastic strain distribution through the thickness of a cold formed metal strip and used this information to validate finite element simulations of the process.

In this paper a new technique for validating roll forming simulations is presented. A sample of the initial flat metal strip was subjected to a tensile load and the extension and load reported. After each extension, the sample was taken off the tensile machine and its hardness was measured. From the permanent extension generated the plastic strain was calculated and this was then related to the hardness. A two dimensional finite element model was created to predict the equivalent plastic strain (PEEQ) in the cross section of the V-band after each roll pass. Only the first stage of the forming process was investigated to keep the results

independent of the band clamp diameter. At the same positions in the roll forming process samples were cut out and the hardness in the cross section was measured using a hardness tester. The previously established relationship between plastic strain and hardness was then used to compare predicted plastic strain values from the finite element model with measured hardness values from the experiments.

# 2   Finite Element Model of Plastic Deformation

## 2.1   *General Set Up of Model*

The Finite Element Analysis package ABAQUS (v6.7) was employed to simulate the cold roll forming process to manufacture V-band clamps. To make the analysis independent of the clamp diameter only the first stage incorporating six passes were set up, only analysing one half as the process has a symmetry. The strip was modelled using three different mesh densities with 12x90, 24x180, and 48x360 equally spaced 2 dimensional reduced integration linear plane strain elements (CPE4R). The analysis was carried out in an implicit static environment and, as undertaken by Papeleux and Ponthot (2002) for a similar 2 dimensional forming process, a penalty algorithm was used to enforce contact. All tools and contact interactions were removed after every pass to include the effect of springback. Papeleux and Ponthot (2002) state that the results obtained for explicit and implicit solver were only slightly different but CPU costs for the explicit solver were almost 60 times higher than for its implicit counterpart. This analysis was generated in two dimensions because although the rolling process is 3 dimensional, the final state of each rolling pass is achieved on a plane. Linear Elements had to be used since as described by Konter (2000) in ABAQUS second-order quadrilateral elements at the contact surface will transfer the contact-force/pressure non- uniformly, sharing 1/6 on each corner node and 2/3 for each middle node. Moreover, Bui et al. (2004) found linear elements with reduced integration to be very suitable for metal forming processes including large bending and large plastic strains, and compared to their fully integrated counterparts, do not suffer from shear locking.

Within the finite element simulation each pass consisting of a pair of rollers was modelled using analytical rigid bodies representing a surface. The rollers were therefore not meshed. The contact between the rollers and the band was simulated using surface-to-surface interactions. No friction was assumed because this would add extra surface stress and strains as the rigid rollers slide over the surface, whereas in the real process the rollers do not slide over the band surface in the vertical direction. All upper rollers were prevented from moving in any direction by applying a boundary condition at their reference points, whereas

the lower rollers where moved upwards pushing the band against their upper counterpart until the distance between the rollers in the simulation matched the clearance in the real rolling process. The clearance between the rollers is the same as the thickness of the initial flat strip.

## 2.2 Material Properties

The material used was AISI 304 stainless steel quarter hard, with experimentally determined values for Young's Modulus of 227 GPa, Poisson's Ratio of 0.29, yield stress of 648 MPa and an ultimate tensile strength of 857 MPa, taken from Shoghi et al. (2004). For the FE-Analysis the material was defined to be elastic-plastic with linear hardening, as also used in the study of Kiuchi (1973) and with a von-Mises yield function as mentioned in Dixit and Dixit (2008). Using equations (1), (2), and (3) all engineering values were transformed into true values for the yield stress $\sigma_{ty}$ and ultimate tensile strength $\sigma_{tUTS}$, and the plastic behaviour could be calculated as described by Tehrani et al. (2006) and Meyers and Chawla (1999).

$$\sigma_t = \sigma_e(1+\varepsilon_e) \qquad (1)$$

$$\varepsilon_t = \ln(1+\varepsilon_e) \qquad (2)$$

$$\varepsilon_{pl} = \varepsilon - \varepsilon_{el} \qquad (3)$$

The complete strain hardening curve and all engineering stress and strain values are shown in Figure 2.
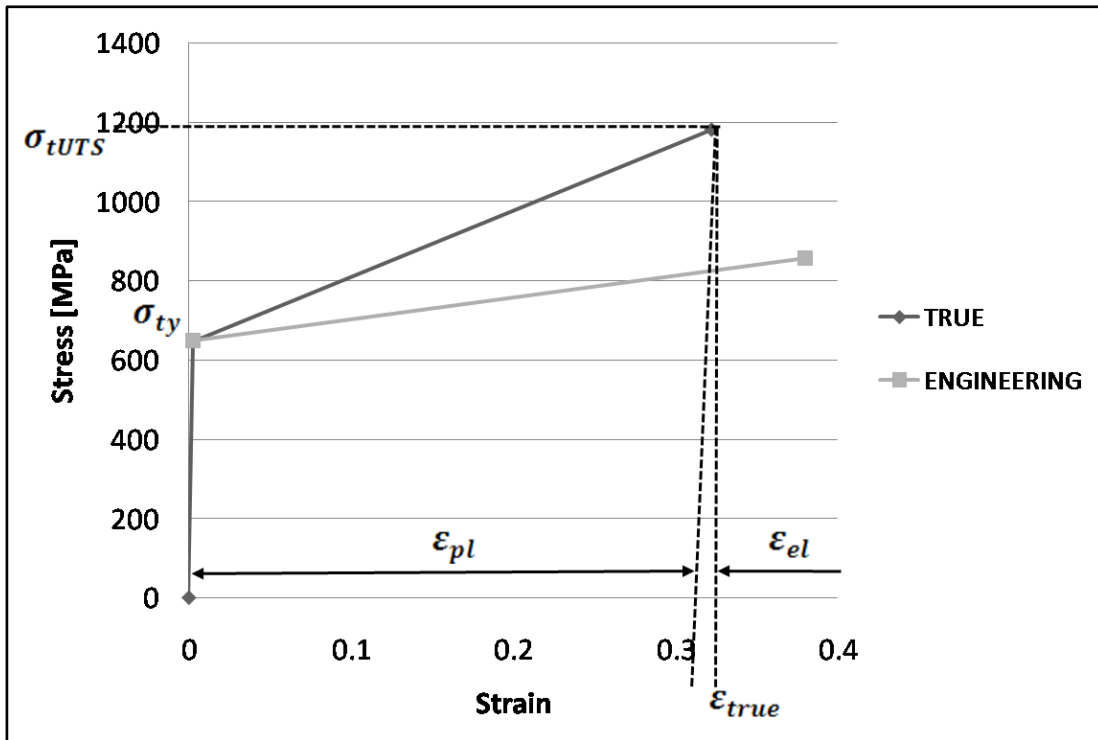
Figure 2: Material model used for finite element simulation

## 2.3  Finite Element Results

### 2.3.1  Mesh Convergence Study

The predicted equivalent plastic strain (PEEQ) in each of the six roll passes for a finite element model with a mesh density of 12x90 elements can be seen in Figure 3. The simulation clearly shows a large increase in plastic strain in the bent areas, and first noticeable in the 4th pass, plastic deformation along the neutral line in the straight part of the clamp leg. As the mesh deformation shows, this latter deformation is due to shear stresses acting in this area.
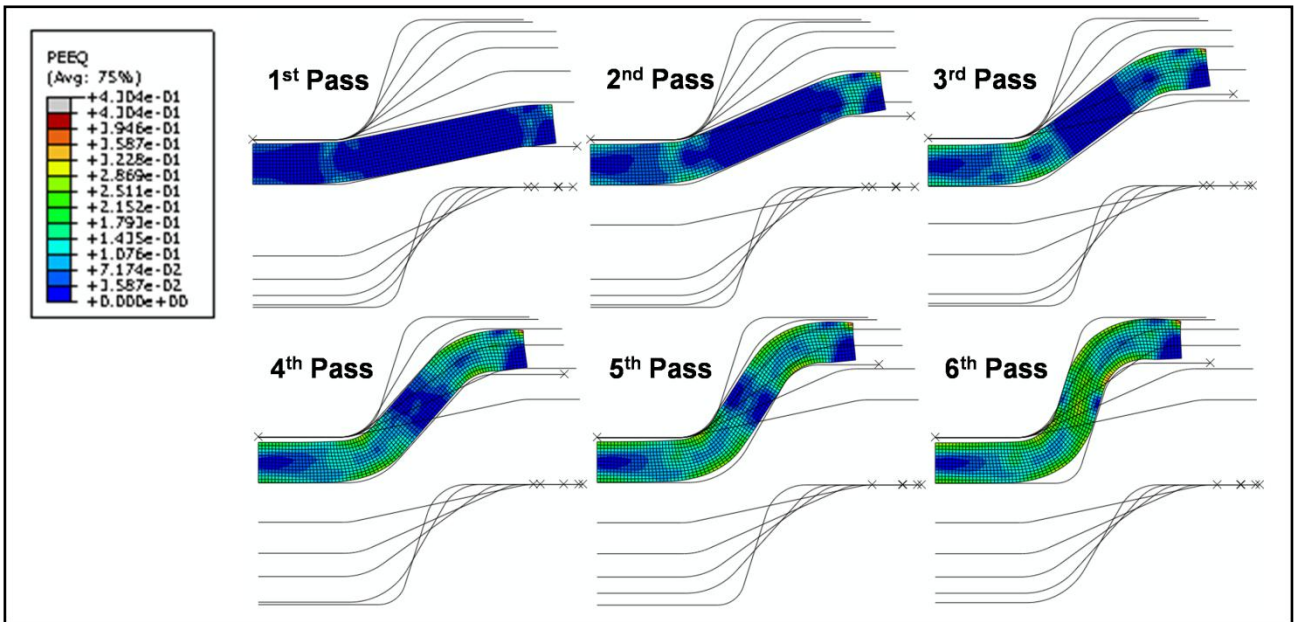
Figure 3: Equivalent plastic strain (PEEQ) in each roll pass for a 12x90element mesh

In order to demonstrate the accuracy and correctness of the initial mesh density with 12x90 elements, a convergence study with two more mesh densities of 24x180 and 48x360 elements was carried out. Three areas in the cross section of the 6th pass were chosen to be compared to each other. These areas were where predicted plastic strain values were compared to measured hardness values to validate the finite element model, as discussed in further detail in section 4. The areas compared in the convergence study are indicated in Figure 4 by red lines through the corner nodes of the elements from which the strain values were extracted. In all three meshes nodes existed along the indicated lines making it possible to make a direct comparison between models.
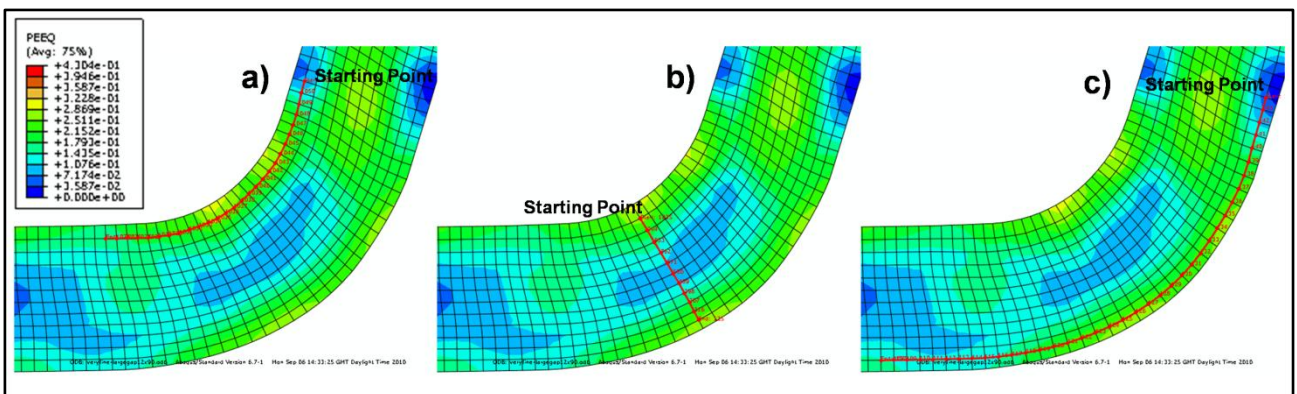


Figure 4: Line of element corner nodes, where plastic strain was reported after 6th pass, a) close to inner surface, b) through the thickness and c) close to outer surface

Figure 5 shows the plastic strain values taken from line a (Figure 4). These results show very good agreement, and only differ slightly between 0.5mm and 1.2mm. As expected, the plastic strain significantly drops at both ends of the red line, as these nodes lie further away from the bent area and either no or very little plastic deformation has taken place. The peaks and valleys visible in the bent area between 0.5mm and 2mm along the line will be discussed further in sub-section 2.3.2.
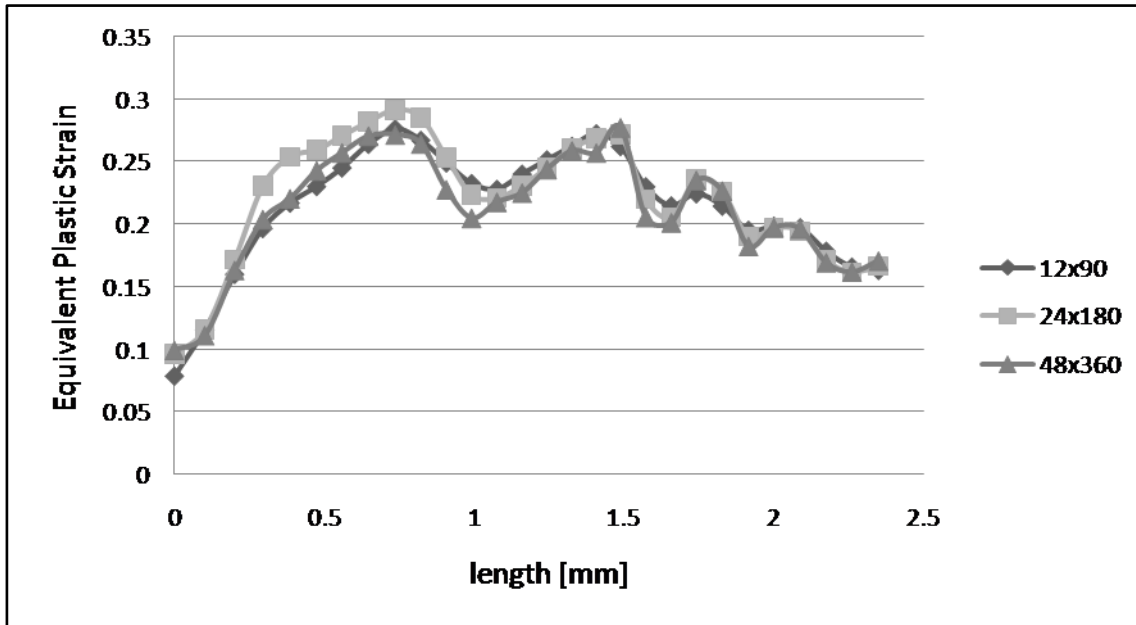


Figure 5: Equivalent plastic strain distribution close to inner surface of the cross section after the 6th pass

The next area of interest was at the outside corner (line c in Figure 4), where mainly tension rather than compression took place. Again reading the plastic strain values taken from the element corner nodes the predicted values are shown in Figure 6. Very good correlation between the results for all mesh densities can be seen, and as in the results for the inner side, the plastic strain drops further away from the bent area, at 0mm and 3.8mm. The two peaks are due to the bending area being slightly shifted to the right of the section (i.e. the left of the graph) as the cold roll forming process progresses, with the peak at 1.1mm being introduced in the 6th pass.
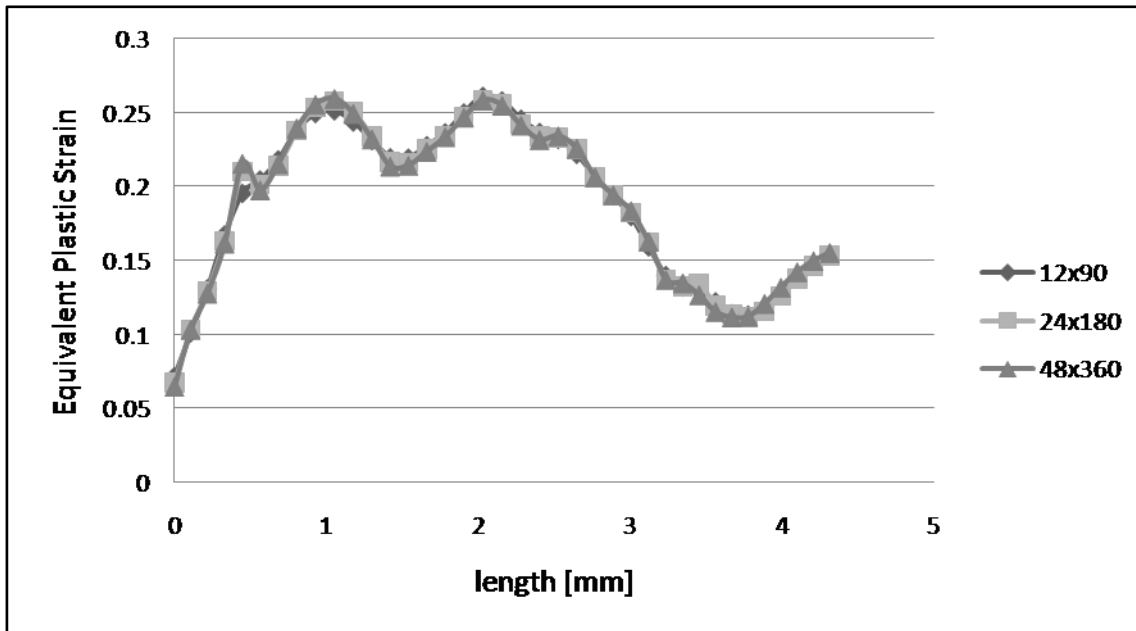
Figure 6: Equivalent plastic strain distribution close to outer surface of the cross section after the 6th pass

The increase in plastic strain between 3.8mm and 4.5mm lies in the nature of the cold roll forming process, as the band is initially bent at the symmetry line as shown in Figure 7shortly before the band gets fully deformed during this first pass. This phenomenon appears throughout all six passes, leading to the plastic strain increasing as well.
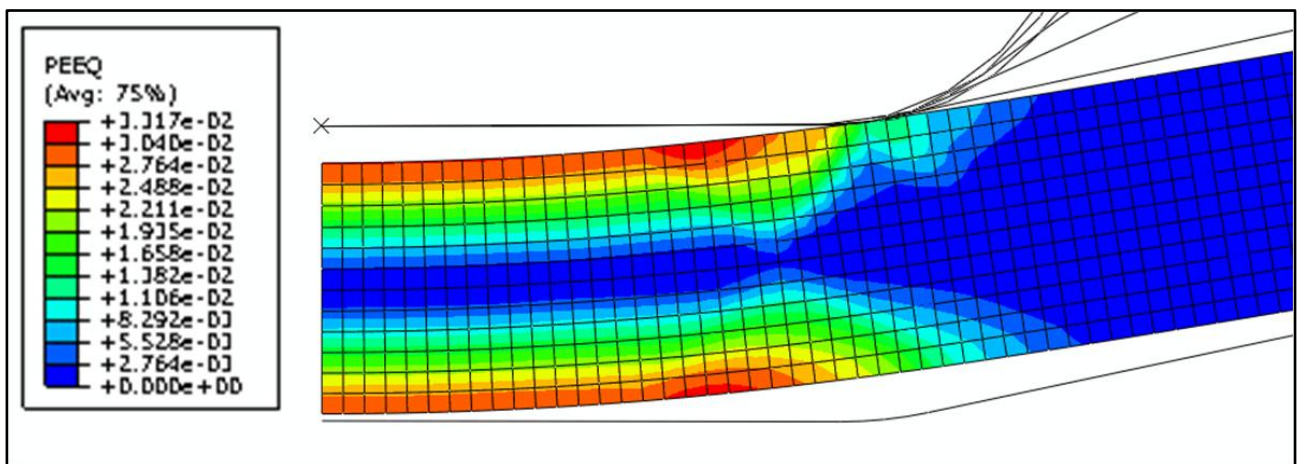


Figure 7: Plastic strain close to the symmetry plane shortly before entering the first pass

The plastic strain distribution through the thickness of the band in the third area investigated in the convergence study , indicated by the red line in Figure 4b, can be seen in Figure 8. The graphs show very good correlation for all mesh densities, and distributions as expected, with very little plastic deformation towards the neutral line halfway through the thickness.
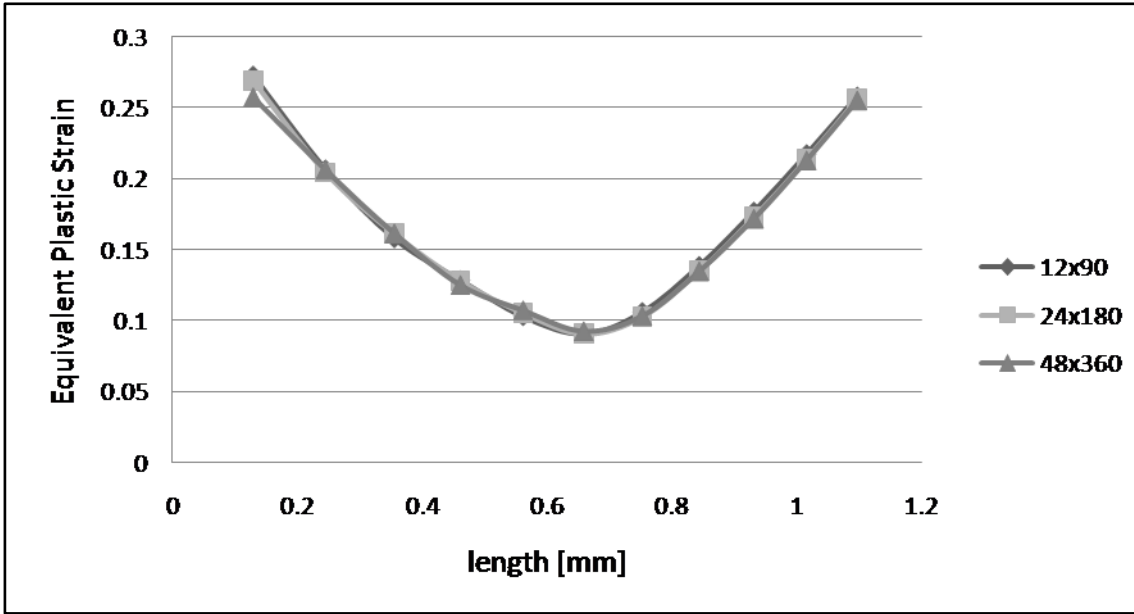
Figure 8: Equivalent plastic strain distribution through the thickness of the cross section after the 6th pass

In all three areas the results shown here demonstrate good convergence after the 6th pass.

## 2.3.2  Influence of Hydrostatic Stress on Plastic Strain Distribution

As described in the previous sub-section, the non-uniform distribution of the equivalent plastic strain (PEEQ) in Figure 5 is worth further investigation. This is of particular interest as Muller and Barrans (2009) have discussed the problem of cracks occurring in this particular area of the inner surface of V-band clamps assembled to turbochargers for diesel engines.

In the zone of band strip where it is in contact with the upper rollers, the stress distribution consists of three compressive stress components. The first one $\sigma_1$ acting in the plane of the section and parallel to the surface of the strip is largest at the inner surface due to the bending. The second component $\sigma_2$ acts out of the plane as 2 dimensional plane strain is assumed and in this area the compressive bending strain would cause material in a short section to expand out of plane. The third compressive stress $\sigma_3$ is due to the contact force between upper roller and band strip. Considering the yield surface geometrically representing the von Mises yield criterion (also see Dixit and Dixit 2008) the first two components $\sigma_1$ and $\sigma_2$ on their own would pass the yield surface leading to material yielding in this zone and significantly increasing the plastic strain. The stress component $\sigma_3$ due to the contact pressure however, acts in the perpendicular direction to the plane represented by $\sigma_1$ and $\sigma_2$, and brings the material closer towards the yield surface, significantly reducing plastic strain. This phenomenon can be seen several times in this cold roll forming process such as in Figure

9a. Here two large peaks in plastic strain appear on both sides of the contact zone with the upper roller during pass 1. Figure 9b shows a peak in the hydrostatic stress (termed "pressure" in ABAQUS), at the contact zone due to the large contact force. For the first pass, this larger hydrostatic stress indicates the correctness of the theory, in which the stress due to contact leads to less plastic deformation.
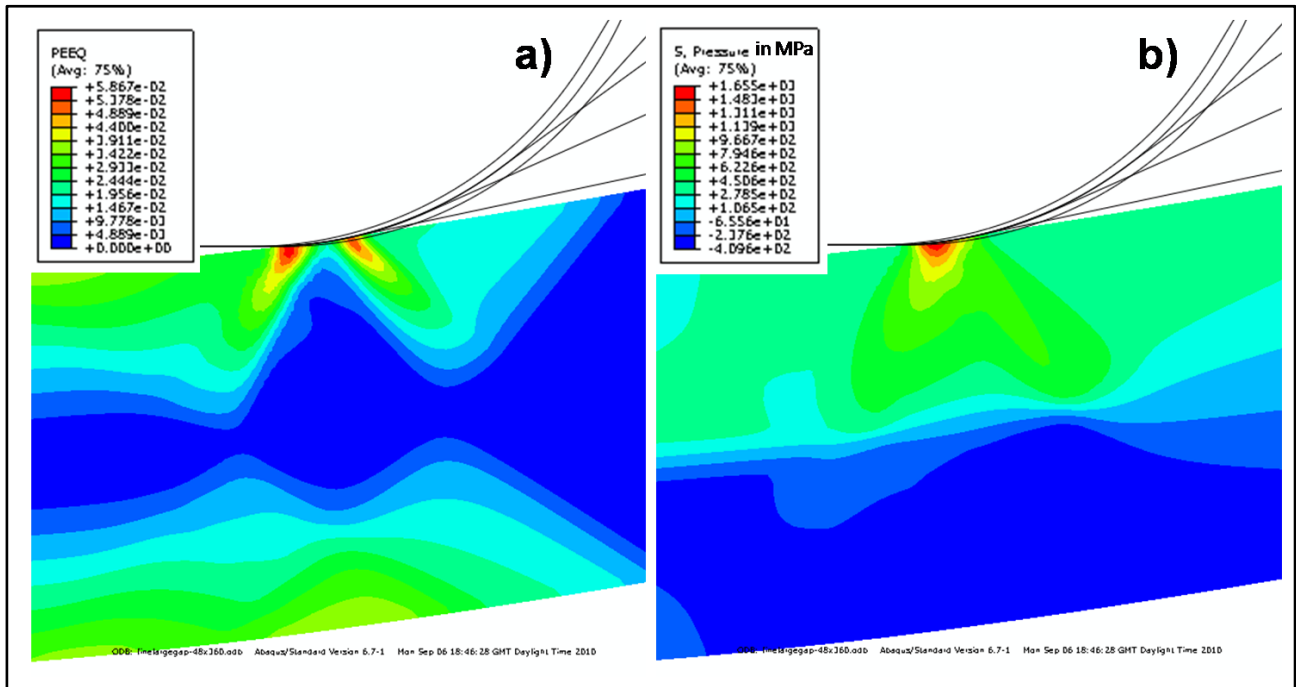


Figure 9: Band strip in contact with upper roll 1 before being fully deformed, a) equivalent plastic strain (PEEQ), b) stress component due to contact force of roller

For the second roll pass, the same tendency can be observed as Figure 10a shows not only two peaks in plastic strain next to the contact zone, but also another third peak left from pass one. Again the two peaks in plastic strain are next to the high hydrostatic stress zone, shown in Figure 10b.
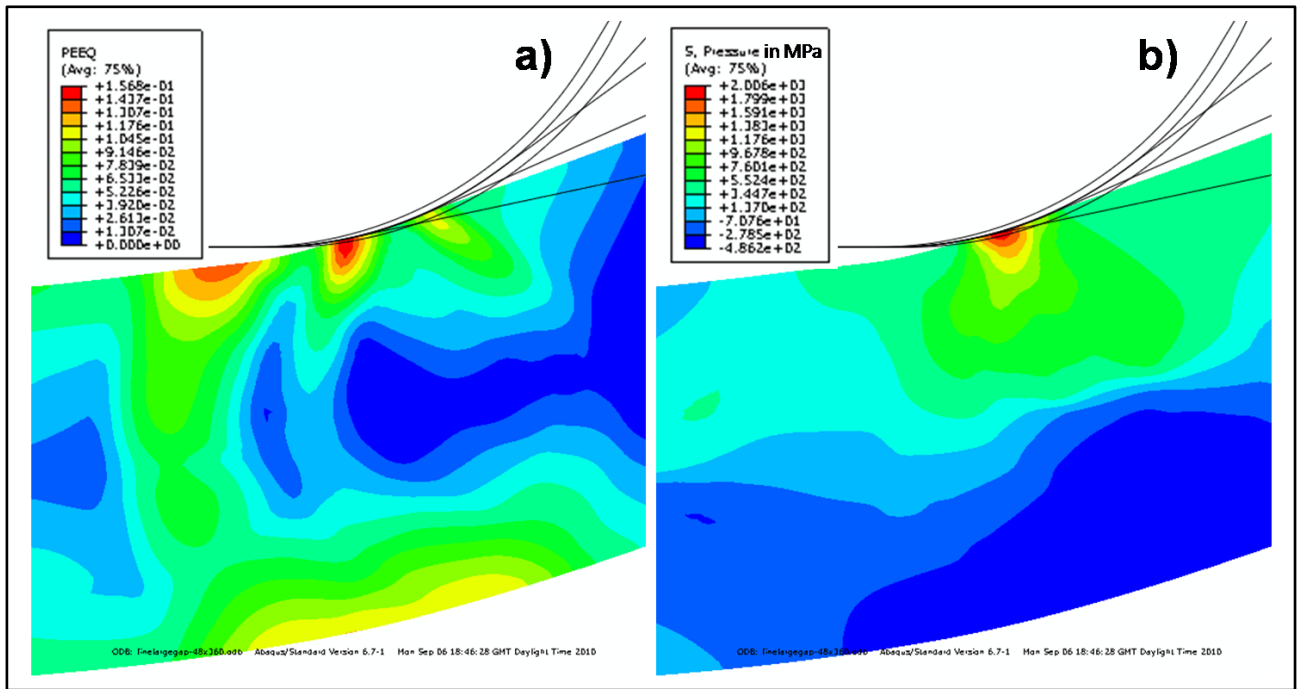
Figure 10: Band strip in contact with upper roller 2 before being fully deformed, a) equivalent plastic strain (PEEQ), b) stress component due to contact force of roller

In Figure 11a, several peaks in plastic strain can be observed at the inner surface of band cross section. The largest peak in plastic strain of 0.29 is generated from the contact in the first and second passes, and the next slightly smaller peak of 0.1995 is generated from the contact interaction in the second, third and fourth passes. The final strain peak of 0.1711 is the second part due to the contact in pass 4, which is clearer when taking into account the large hydrostatic stress in Figure 11b.
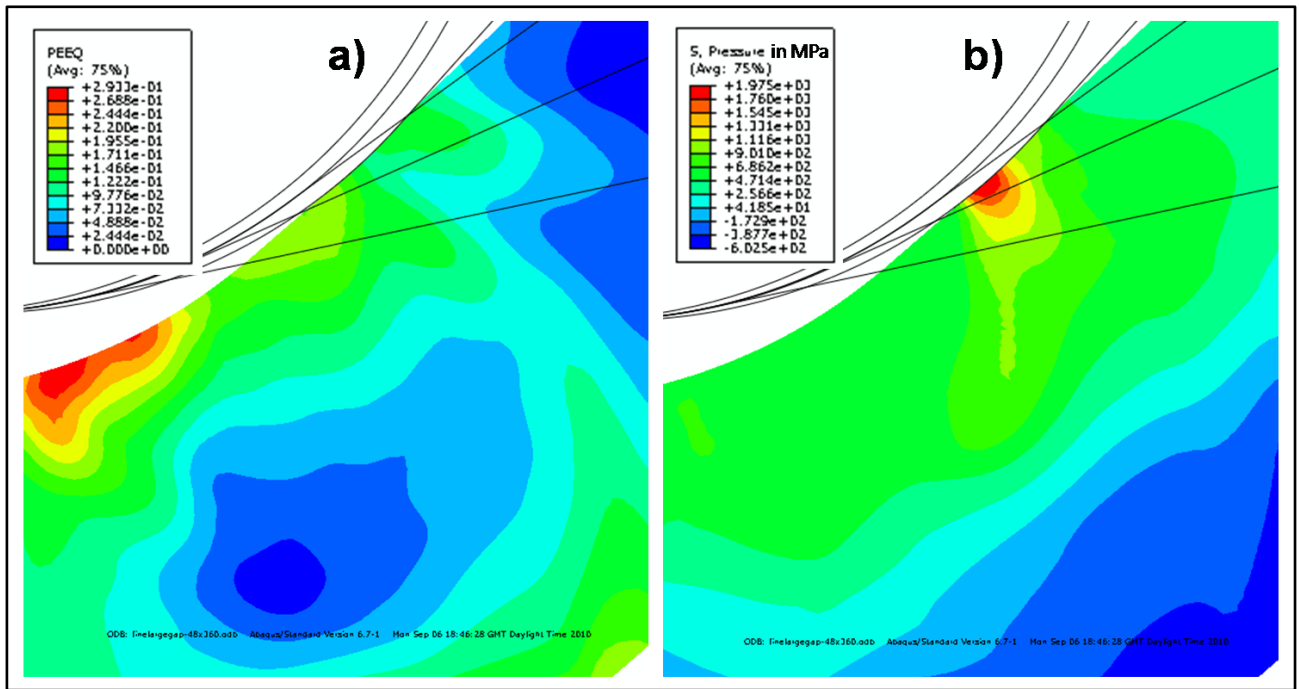
Figure 11: Band strip in contact with upper roller 4 before being fully deformed, a) equivalent plastic strain (PEEQ), b) stress component due to contact force of roller

The two dimensional finite element model clearly showed that in a plane strain case with bending acting, stresses due to the contact force can significantly reduce the plastic deformation this area.

# 3 Experimental Testing

## 3.1 Methods

A tensile test for austenitic stainless steel AISI 304 was carried out to establish data to validate the finite element simulations described above. Using a tensile test machine a standard test sample of the initial flat band was extended in increments of plastic strain. The sample was taken off the machine to measure the work hardness (HMV) at each increment. All hardness measurements used the Vickers hardness scale and were taken using a Microhardness Tester Buehler 1600-6100. For the tensile tests specimens, care was taken to ensure that the sample had not started to neck before measurements were taken.

The second set of hardness measurements can be sub-divided into two categories. The first showed the increase in work hardness throughout the cold roll forming process starting from the initial flat band to a sample of the sixth roll pass. The second was used to establish a new method to validate the finite element results for the sixth pass. For both categories the hardness was measured at several points through the

cross-section of the band perpendicular to the rolling direction. The samples were obtained by taking a strip out of the roll forming machine including all six passes. The position of each pass was marked on the strip and after that small samples were cut off the string close to each marked position. Figure 1 shows at which positions the samples were taken from. Figure 12 gives an overview of the measuring points in the cross-section for the final forming stage, pass 6.
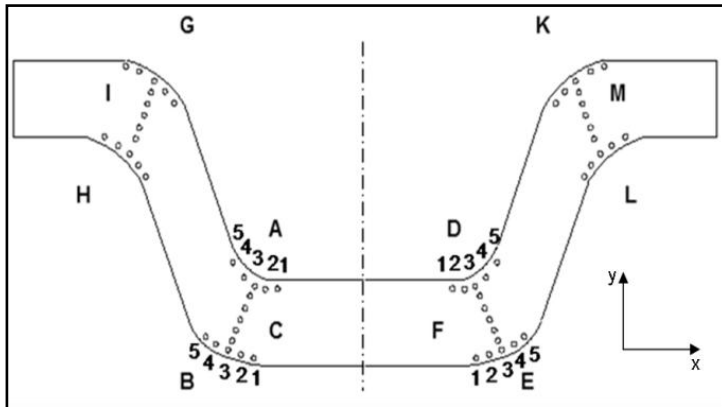


Figure 12: Work Hardness measuring points to show increase throughout roll forming process (6th pass)

The regions measured in the cross-section, A to M were chosen because the finite element results showed large changes in plastic deformation, so these are likely to have the largest change in hardness through the forming process. The points of regions A, B, D, E, G, H, K and L were measured with a distance to the outside surface between 0.08 and 0.15mm. Using an optical microscope with a micro adjustable x-y stage on the hardness machine, the position of the right and left hand side of each sample was set. It was then possible to define the plane of symmetry and from there the x-distance to each point was defined. A similar process using the upper and lower edges of the samples was used to define the y-coordinate for each point. Considering that each machining process has certain tolerances it was not possible to measure the hardness of a specific point at exactly the same position for each pass. This paper focuses especially on regions A, B, C, D, E, and F, as they are expected to have the largest impact on the actual strength of the joint and crack development in the V-band cross section. Five measuring points in each region were assumed to be sufficient to show the work hardness progression, whereas between 6 and 16 points were required to establish an accurate validation for the finite element work, as shown in Figure 13.
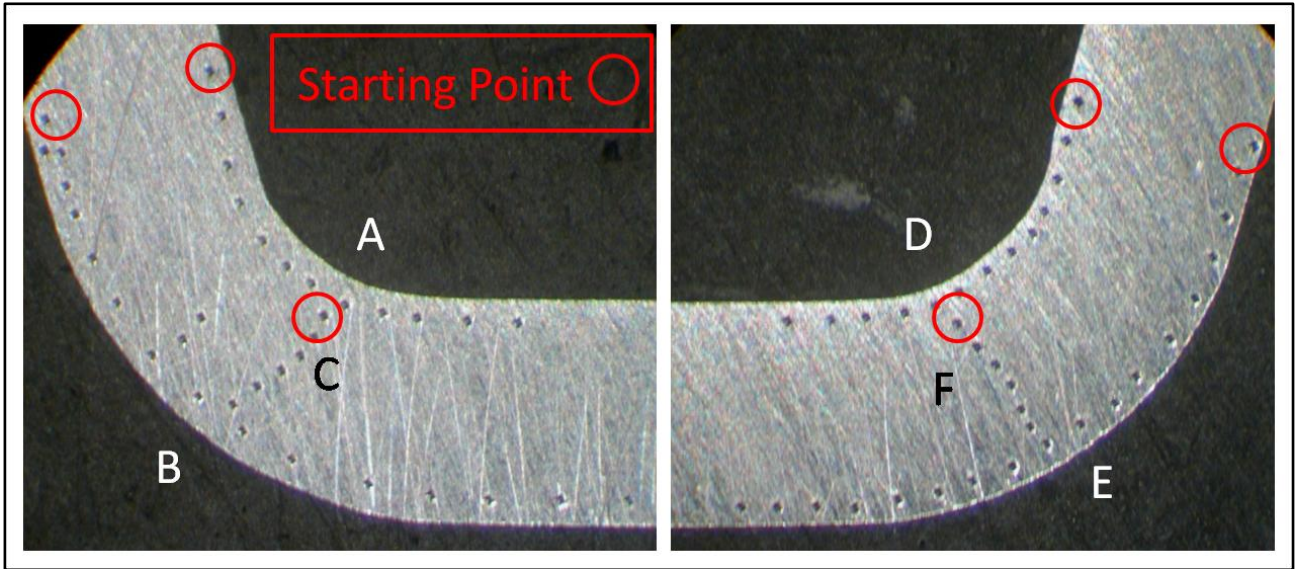
Figure 13: Work Hardness measuring points for validating finite element analyses (6<sup>th</sup> pass)

## 3.2 Results

### 3.2.1 Tensile and Hardness Test to establish Validation Method

Using equations (1), (2), and (3) and undertaking the same procedure as for the finite element model, all engineering values gathered from the tensile test sample were transformed into true values and the plastic behaviour could be calculated. This allowed the relationship between plastic strain and work hardness to be established, as shown in Figure 14.
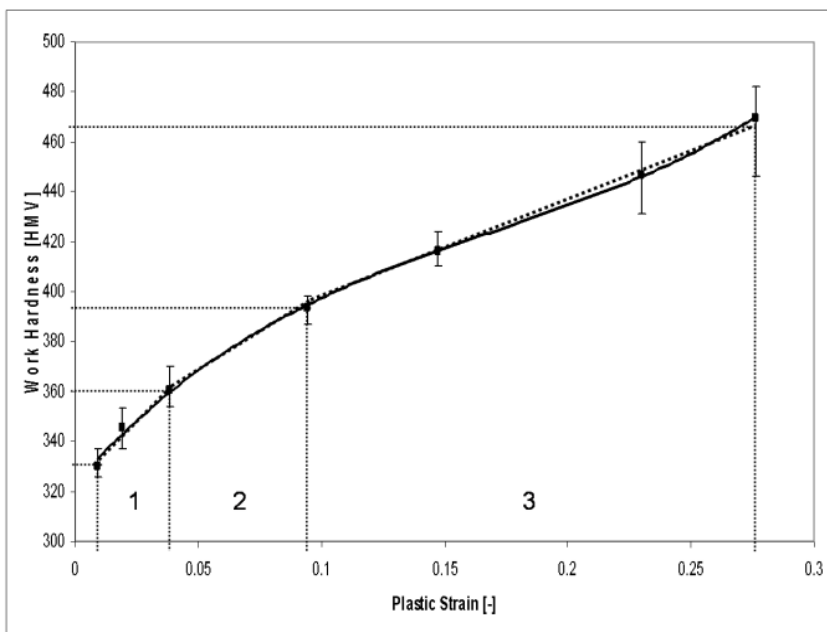


Figure 14: Correlation between work hardness and plastic strain for AISI 304

The hardness values in Figure 14 were determined for plastic strain values between 0.009 and 0.0277 and then partially linearised (dashed lines) in three regions, generating equations (4) to (6):

Region 1          $0.009 \leq \varepsilon_{pl} < 0.039$:

$$H_1 = \varepsilon_{pl} \times 1000 + 320 \qquad (4)$$

Region 2          $0.039 \leq \varepsilon_{pl} < 0.095$:

$$H_2 = \varepsilon_{pl} \times 643 + 336 \qquad (5)$$

Region 3          $0.095 \leq \varepsilon_{pl} < 0.277$:

$$H_3 = \varepsilon_{pl} \times 362 + 360 \qquad (6)$$

## 3.2.2  Determination of Work Hardness throughout Cold Roll Forming Process

Figure 15 to Figure 17 display the experimental results for the development of work hardness in three regions through the six pass roll forming process. The ordinate shows the Vickers Hardness and the abscissa the number of the sample point. Figure 15 indicates that for region A the greatest work hardening is in the centre of the fillet. This is the area predicted by the FE analysis as having the largest plastic deformation. The further away the sample points are from the centre, the smaller is the work hardness. Only the graph for the initial flat band has a relatively constant value of hardness taking account of measurement uncertainty.
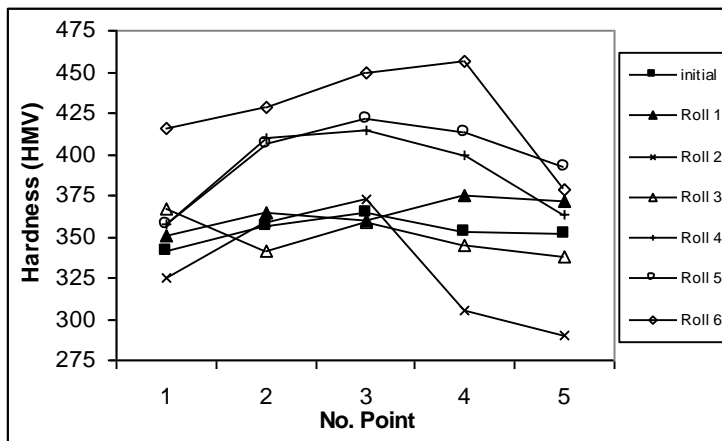
Figure 15: Hardness measured at region A (all passes)

The behaviour observed for region A can also be seen for area B in Figure 16. The largest magnitude of hardness occurred at the centre of the fillet indicated as number 3. Again, this is where the FE analysis predicts the largest plastic strain.
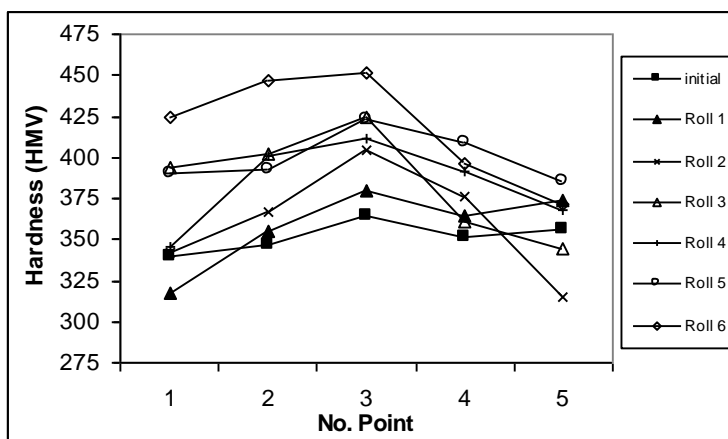


Figure 16: Hardness measured at region B (all passes)

The graphs in Figure 17 show the development of work hardening through the thickness of the band in region C. The graph for the initial flat band indicates that the band has already had a range of hardness through the thickness, with the magnitude decreasing towards the neutral plane. This range was due to the preceding flat rolling process. As the graphs for the six pairs of rollers display, this trend develops further as the band undergoes more deformation.
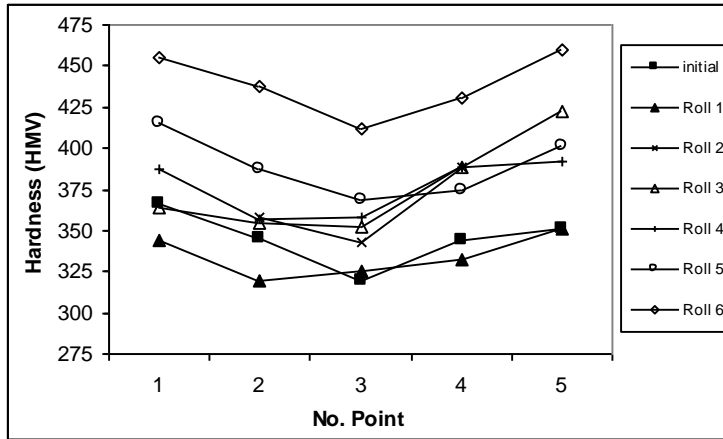
Figure 17: Hardness measured at region C (all passes)

The trends shown by the experimental results obtained in this investigation agreed with the numerical results obtained from FE analysis. In order to get a quantitative comparison a further experimental investigation was undertaken to relate work hardness and plastic strain directly.

# 4 Experimental Validation

Using the relationship established in sub-section 3.2.1, it was then possible to convert the plastic strain values found by the FE analysis into hardness values. The transformed numerical hardness results taken from pass six were then compared to the measured hardness values at regions A, B, C, D, E, and F.

The Hardness values for areas A and D (see Figure 4 and Figure 13) determined in the experimental tests compared to their numerical counterparts (48x360 element mesh) are shown in Figure 18. The values for the hardness are shown over the length as the distance between the points was measured, starting at zero with the point at the top of the areas A and D. The same was done for the finite element results, but there the distance between the nodes was taken as the length value. As indicated, these values correlate with each other very well showing the largest magnitude in the centre of the fillet. The overall trend of the measured hardness fits well with the predicted results, especially for the parts between 0mm and 1mm. and 2mm to 2.5mm. In between 1mm and 2mm, it can be noticed that the overall trend, as well as the absolute hardness values seem to deviate and do not show the best correlation. This may be due to uncertainties when measuring the x- and y-distance of each point. The V-section angle was assumed to be 37° in the sixth pass as specified for the component. However the manufacturing process has an associated tolerance and in the current experiments, the angle of the V-section was not initially measured. An additional difficulty found in

this method was accurately controlling the position of the hardness points relative to the surface and hence to specific points on the finite element simulation.
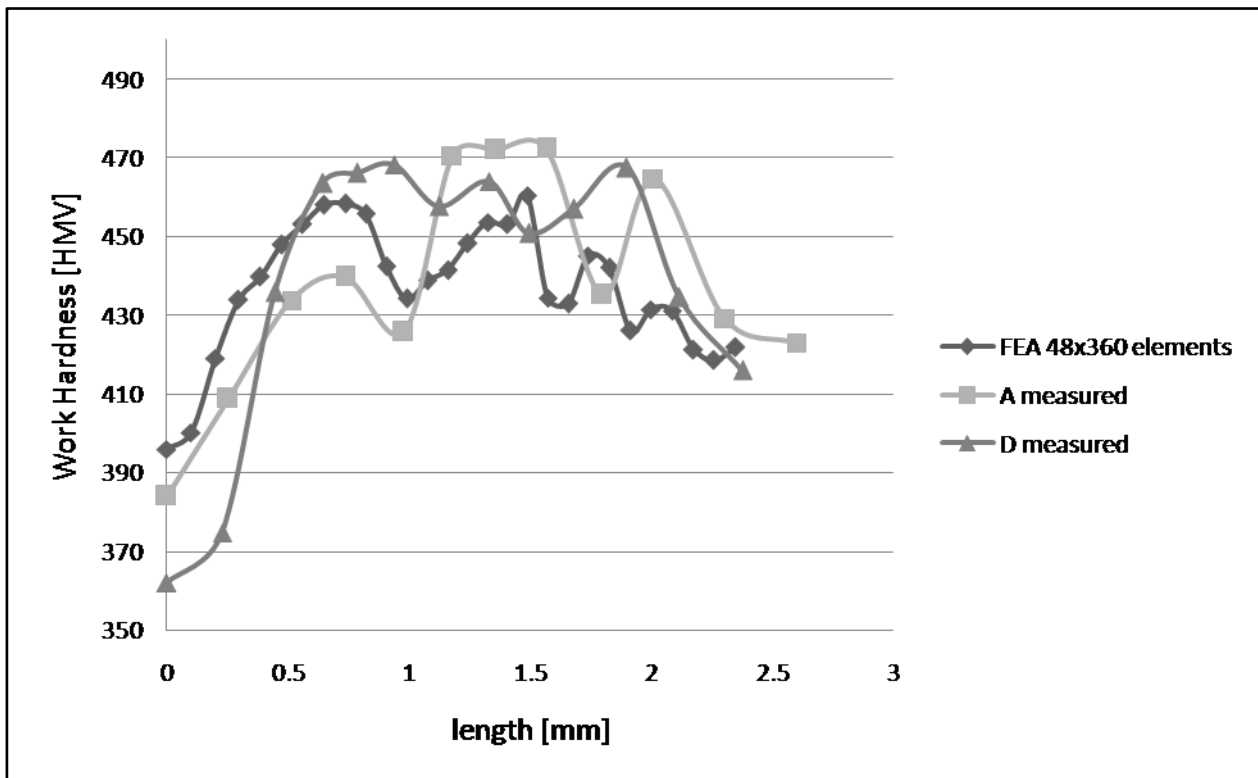


Figure 18: Comparison of Hardness determined for regions A, D and Hardness obtained by predicting plastic strain (6th pass)

The same good correlation for the overall trend of measured areas B and E compared to the finite element results can be seen in Figure 19, with the peaks in the centre of the fillet. As for areas A and D, also here very good correlation can be seen for results between 0mm and approximately 1.5mm. From 1.5mm onwards the results for area F give a better fit to the numerical results than area B. However, the decrease of the hardness further away from the bent area can be seen for both regions. Again, the absolute values for the measured and predicted hardness values differ from 1.5mm.
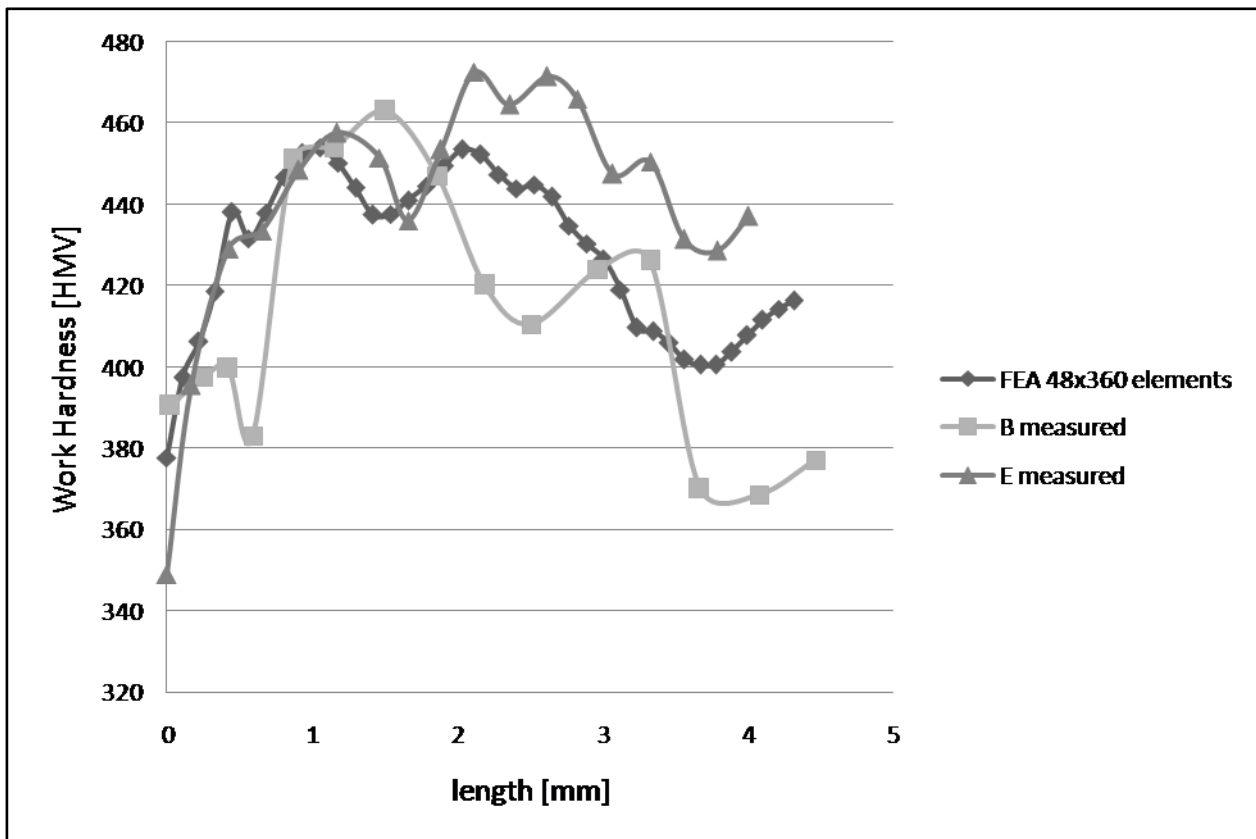
Figure 19: Comparison of Hardness determined for regions B, E and Hardness obtained by predicting plastic strain (6th pass)

Very good correlation in the overall trend as well as the absolute values between predicted and measured hardness for regions C and F can be observed from Figure 20. All three graphs show the expected distribution through the thickness of the cross section as a parabola, with the hardness values decreasing towards the neutral line.
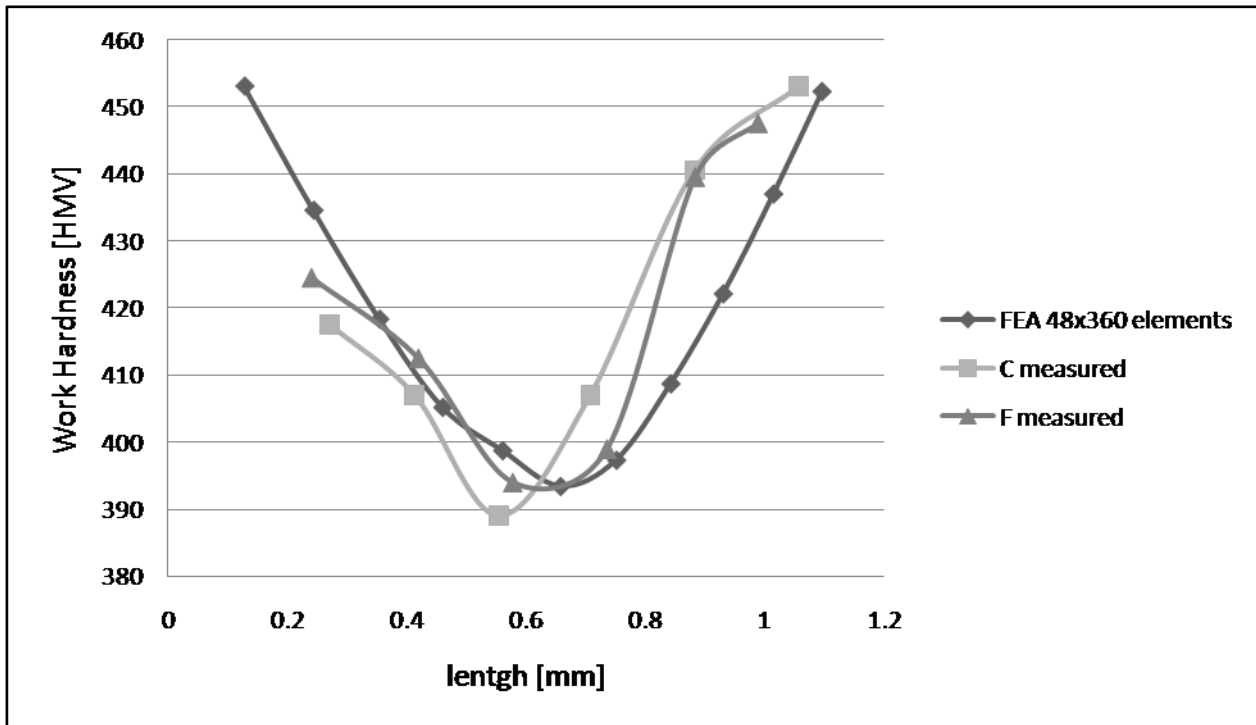
Figure 20: Comparison of Hardness determined for regions C, F and Hardness obtained by predicting plastic strain (6th pass)

Although the experiments carried out in the presented work have shown partial deviations between predicted and measured hardness, it is clear that validating predicted plastic strain in finite element analysis by measuring the work hardness is useful technique.

# 5  Conclusion

In this paper, a new method of validating finite element predictions has been demonstrated. Compared to more classical methods of measuring plastic strain, such as the cutting and hole drilling technique, the method presented in here does not apply strain gauges, but operates by measuring the work hardness with a hardness tester and uses information gathered from a tensile test. Moreover, the classical use of strain gauges only measures the surface strain. Whilst for thin metal sheets this technique provides enough data, it does not deliver enough information about the plastic deformation for thicker cross sections in which shear stresses have greater effects. As crack growth is more severe in thicker metal sheets, the additional, more detailed information gathered by the presented method of measuring the actual hardness may be important for investigating the development of cracks and improving the roll forming process. The finite element work

has also shown significant changes in plastic deformation in the bent area and correlates with measurements very well.

In addition to employing a new method of validating finite element results, the development of work hardness throughout the cold roll forming process of manufacturing V-band clamps has been investigated. The results showed good agreement with existing knowledge in the field. The overall trend showed hardness increasing in areas where plastic deformation has taken place.

# 6    Further Work

In future, the knowledge obtained in this paper can be used to investigate the behaviour of V-band clamps when assembled to a pair of flanges and sustaining an axial load. To achieve this, a 3D FE-Analysis of the roll forming process (including the 7th ring forming stage) should be carried out to generate a model of V-band containing the plastic strains generated during manufacturing. This model could then be assembled to a model of a pair of flanges. Simulating an axial load using this combined model would greatly enhance understanding of the failure mode of V-band clamps of different sizes.

## Acknowledgement

## References

Barrans, S.M., Muller, M., 2009. Finite element prediction of the ultimate axial load capacity of V-section band clamps. In: 7th International Conference on Modern Practice in Stress and Vibration Analysis, Cambridge, UK.

Bhattacharyya, D., Smith, P. D., Yee, C. H., Collins, I. F., 1984. The Prediction of Deformation Length in Cold Roll-Forming. Journal of Mechanical Working Technology 9, 181-191.

Bui, Q.V., Papelux L., Ponthot, J.P., 2004. Numerical simulation of springback using enhanced assumed strain elements. Journal of Materials Processing Technology 153-154, 314-318.

Bui, Q.V., Ponthot, J.P., 2008. Numerical simulation of cold roll-forming processes. Journal of Materials Processing Technology 202, 275-282.

Cruise, R.B., Gardner, L., 2008. Residual stress analysis of structural stainless steel sections. Journal of Constructional Steel Research 64, 352-366.

Dixit, P.M., Dixit, U.S., 2008 Modeling of Metal Forming and Machining Processes by Finite Element and Soft Computing Methods, Springer, London, pp.101.

Han, Z. W., Liu, C., Lu, W. P., Ren, L. Q., 2002. Simulation of a multi-stand roll-forming process for thick channel section. Journal of Materials Processing Technology 127, 382-387.

Han, Z. W., Liu, C., Lu, W. P., Ren, L. Q., Tong, J., 2005 Spline finite strip analysis of forming parameters in roll forming a channel section. Journal of Materials Processing Technology 159, 383-388.

Heislitz, F., Livatyali, H., Ahmetoglu, M. A., Kinzel, G. L., Altan, T., 1996. Simulation of roll forming process with the 3-D FEM code PAM-STAMP. Journal of Materials Processing Technology 59, 59-67

Hong, S., Lee, S., Kim, N., 2001. A parametric study on forming length in roll forming. Journal of Materials Processing Technology 113, 774-778.

Kain, V., Chandra, K., Adhe, K.N., De, P.K. 2004. Effect of cold work on low-temperature sensitization behavior of austenitic stainless steel. Journal of Nuclear Materials 334, 115-132.

Kim, W., Kawai, K., Koyama, H., Miyazaki, D., 2007. Fatigue strength and residual stress of groove-rolled products. Journal of Materials Processing Technology 194, 46-51.

Kiuchi, M., 1973. Analytical study on cold roll forming process. Report of Inst. Ind. Sci. University of Tokyo 23.

Kiuchi, M., Koudabashi, T., 1984. Automated design system of optimal roll profiles for cold roll forming. In: Bedford, Editor , Proceedings of the Third International Conference on Rotary Metalworking Processes, Kyoto, Japan, p. 423-436.

Kleiner, M., Krux, R., Homberg, W., 2004. Analysis of Residual Stresses in High-Pressure Sheet Metal Forming. CIRP Annals-Manufacturing Technology 53 (1), 211-214

Konter, A., How to – Undertake a Contact and Friction Analysis, NAFEMS, Glasgow, pp. 11-13.

Kumar, B.R., Singh, A.K., Das, S., Bhattacharya, D.K. 2004. Cold rolling texture in AISI 304 stainless steel. Materials Science and Engineering A 364(1-2), 132-139.

Lindgren, M., 2005. Finite element model of roll forming of a U-channel profile. In: International Conference on Tech. of Plasticity, Verona.

Lindgren, M., 2007a. Cold roll forming of a U-channel made of high strength steel. Journal of Materials Processing Technology 186, 77-81.

Lindgren, M., 2007b. An improved model for the longitudinal peak strain in the flange of a roll formed U-channel developed by FE-analysis. Steel Res. Int. 78(1), 82-87.

McClure,C.K., Li,H., 1995. Roll Forming Simulation using Finite Element Analysis. Manufacturing Review 8, 114-119.

Meyers, M.A., Chawla, K.K., 1999. Mechanical Behavior of Materials, London, pp. 116

Milad, M., Zreiba, N., Elhalouani, F., Baradai, C., 2008 The effect of cold work on structure and properties of AISI 304 stainless steel. Journal of Materials Processing Technology 203, 80-85.

Mountford, R., 1980. Design of clamp joints. Engineering Designer, 37-39.

Muller, M., Barrans, S.M., 2009. Ultimate Axial Load Capacity of V-Band Clamp Joints. In: University of Huddersfield (Ed.), Proceedings of Computing and Engineering Annual Researchers' Conference, Huddersfield, UK, 14-18

Muller,M., Barrans,S.M., 2010. Impact of flange geometry on the ultimate axial load capacity of V-band clamps. In: 9th International Conference on Turbochargers and Turbocharging, London, UK.

Panton, S. M., Duncan, J. L., Zhu, S. D., 1996. Longitudinal and shear strain development in cold roll forming. Journal of Materials Processing Technology 60, 219-224.

Papeleux, L., Ponthot, J.-P., 2002. Finite element simulation of springback in sheet metal forming. Journal of Materials Processing Technology, 785-791.

Paralikas, J, Salonitis, K., Chryssolouris, G., 2009. Investigation of the effects of main roll-forming process parameters on quality for a V-section profile from AHSS. International Journal of Advanced Manufacturing Technology 44, 223-237.

Paralikas, J., Salonitis, K., Chryssolouris, G., 2010. Optimization of roll forming process parameters - a semi-empirical approach. International Journal of Advanced Manufacturing Technology
47, 1041-1052

Quach, W.M., Teng, J.G., Chung, K.F., 2006. Finite element predictions of residual stresses in press-braked thin-walled steel sections. Engineering Structures 28, 1609-1619.

Shoghi, K., 2003. Stress and Strain Analysis of flat and V-section band clamps. University of Huddersfield: Huddersfield.

Shoghi, K., Barrans, S.M., Rao, H.V., 2004. Stress in V-section band clamps. J. Mech. Eng. Sci. 218, part C, 251-261.

Shoghi, K., Barrans, S.M., Rao, H.V., 2003. Classical and finite element analysis of V-band retainers. In: NAFEMS World Congress, Orlando, Florida, USA.

Shoghi, K., Barrans, S.M., Ramasamy. P., 2006. Axial load capacity of V-section band clamp joints. In: 8th International Conference on Turbochargers and Turbocharging, London, UK, pp. 273-285

Tehrani, M.S., Hartley., P., Naeini, H.M., Khademizadeh, H., 2006. Localised edge buckling in cold roll-forming of symmetric channel section. Thin-walled structures 44, 184-196.

Weng, C.C., Pekoz, T., 1990. Residual stresses in cold-formed steel members. Journal of Structural Engineering 116 (6), 1611-1625.

Weng, C.C., White, R.N., 1990a. Residual stresses in cold-bent thick steel plates. Journal of Structural Engineering 116 (1), 24-39.

Weng, C.C., White, R.N., 1990b. Cold-bending of thick high-strength steel plates. Journal of Structural Engineering 116 (1), 40-54

Zeng, G., Li, S.H., Yu, Z.Q., Lai, X.M., 2009. Optimization design of roll profiles for cold roll forming based on response surface method. Materials and Design 30(6), 1930–1938

Zhang, L., Tan, N., Liu, C., 2010. A New Model for Simulation of Cold Roll-Forming of Tubes by Using Spline Strip Method. Journal of Shanghai Jiaotong University 15 (1), 70-75

Zhu, S.D., Panton, S.M., Duncan, J. L., 1996. The effects of geometric variables in roll forming a channel section. Proc. Inst. Mech. Engrs. 210, 127-134.